Alternate rotating walls for thermal chaotic mixing

Kamal El Omari, Yves Le Guer

Alternate rotating walls for thermal chaotic mixing

Kamal El Omari[a,*], Yves Le Guer[a]

[a] *Laboratoire de Thermique Energétique et Procédés (LaTEP)*
Université de Pau et des Pays de l'Adour (UPPA)
Technopole Hélioparc, avenue du Président Pierre Angot, 64053 Pau - France

Abstract

In this study, we numerically investigate the evolution of two-dimensional mixing and heat transfer enhancement within a two-rod stirring device. The fluid is heated by the walls, which are maintained at a constant temperature. We show by analysis of different stirring protocols that the use of discontinuous wall rotations is necessary to promote heat transfer by chaotic mixing. This condition is also required to avoid hot spots in the vicinity of the walls. The statistics of temperature scalars (mean and standard deviation of dimensionless temperature fields) allow us to determine the influence of geometrical and physical parameters on mixing and heating performance. Thermal strange eigenmodes are revealed during the mixing process by the development of complex recurrent patterns, and the self-similar character of temperature evolutions is confirmed by the probability distribution functions of the rescaled non-dimensional temperature.

Key words: Chaotic mixing, Laminar mixing, Heat transfer, High Prandtl number, Thermal eigenmodes, Unstructured finite volume method

Nomenclature

A_c	surface of a mesh element (m^2)
$A_{T\sigma}$	composite mixing indicator
c_p	heat capacity ($J.kg^{-1}.K^{-1}$)
$\vec{d}$	vector joining the centers of two cells
E	energy (J)
k	thermal conductivity ($W.m^{-1}.K^{-1}$)
$\vec{n}$	normal oriented vector
p	pressure (Pa)
R_3	tank radius (m)
R_1, R_2	rod radii (m)
s	strip width (m)
S_{tot}	total surface of the fluid (m^2)
t	time (s)
T	temperature (K)

*Corresponding author, Fax: +33 5 59407160
Email addresses: kamal.elomari@univ-pau.fr (Kamal El Omari), yves.leguer@univ-pau.fr (Yves Le Guer)

U tangential velocity
$\vec{U}$ velocity field ($m.s^{-1}$)
V volume (m^3)
X rescaled dimensionless temperature

Dimensionless numbers

Pe Péclet number
Pr Prandtl number
Re Reynolds number
S_t Strouhal number
T^* dimensionless temperature

Greek symbols

α thermal diffusivity ($m^2.s^{-1}$)
ε eccentricity (m)
ϕ generic scalar variable
Γ generic diffusion coefficient
λ stretching rate (s^{-1})
ρ fluid density ($kg.m^{-3}$)
σ standard deviation
τ period of modulation (s)
$\overline{\overline{\tau}}$ viscous stress tensor
Ω angular velocity ($rd.s^{-1}$)
χ_g scalar temperature dissipation indicator

Subscript

c cell
m mean
f face of a cell

Superscript

$*$ dimensionless

1. Introduction

The topic of heat transfer and mixing plays an important role in many fields as various as earth and life sciences, chemical engineering and material science. This subject is particularly difficult to solve when highly viscous fluids are concerned. A variety of industrial processes involve the heating of highly viscous liquids; they include material processing (molten polymers for example), petroleum engineering, food engineering or environmental engineering. The motivation for this study is to analyze the heating and mixing performance of a chaotic mixer with a rather simple design. Chaotic mixing is obtained by considering the chaotic advection phenomenon [1, 2, 3] that occurs in laminar flow. Today it is well recognized that chaotic mixing is the most efficient mixing process when highly viscous fluids are involved [4]. Chaotic mixing is also recommended for the mixing of delicate fluids that do not resist the high strains encountered in turbulent flows. Despite the simplicity of their velocity fields, chaotic advection flows are able to create very complex patterns of the advected scalar with highly stretched and folded structures. The more numerous are very thin striations produced by the flow, the more efficient the diffusion and the faster the homogenization of the scalar.

When heat transfer is considered, temperature is the scalar and heat conduction is the diffusion source. In the present study we focus only on the relationship between chaotic mixing and the enhancement of heat transfer in a particular flow. Despite its obvious industrial relevance, there are only a limited number of works that consider this problem. In fact, many more works in the literature concern the relationship between chaotic mixing and chemical reaction more than the coupling of chaotic mixing with heat transfer. When heat transfer enhancement is involved, mainly two classes of flow geometries are encountered in the production of chaotic mixing: those that use rotating elements as eccentric cylinders [5, 6, 7, 8] and those that use multiple pipe bends [9, 10, 11, 12, 13, 14, 15, 16, 17, 18, 19]. For the latter geometries, chaotic trajectories are determined by continuous modification of pipe wall design; the third space dimension provides the required additional degree of freedom and no displacement of the wall is imposed. As a consequence, the number of operating parameters that determines the options for effective stirring protocols is reduced, and the flow structure is given only by the chosen pressure gradient (i.e., the Reynolds number for a particular fluid). Another interesting 3D geometry is the continuous chaotic flow generated inside the Rotated Arc Mixer of Lester *et al.* [20]. The mixer consists of an inner stationary cylinder lacking internal structure, with apertures cut through its wall, wrapped by a concentric outer rotating cylinder. This geometry offers a large, tunable, optimization parameter space for the enhancement of heat and/or mass transfer. For all of the cases discussed above, thermal chaotic mixing is used to attain multiple objectives: to encourage heat transfer between the heated walls and the neighboring fluid and to achieve temperature homogeneity for the whole fluid domain. For this last condition, we need to both prevent the formation of a large, unmixed KAM island, where the fluid remains cold, and also avoid hot spots in the vicinity of heated walls, which can degrade the fluid.

One of the main differences between thermal chaotic mixing and reactive chaotic mixing is due to the large contrast in transfer rates between mass and heat. Effectively, it is common to notice a difference of two decades or more between the values of the molecular and thermal diffusivities. Thermal diffusivities are higher than molecular diffusivities, which has consequences on the solutions obtained for the advection-diffusion problem. Typically, the patterns of the *strange eigenmodes* [21, 22] obtained for the scalar fields will differ. These patterns appear repeatedly for periodic velocity fields and repeat themselves every period with an exponential decay of the scalar contrast. More often, asymptotic transport is controlled by the slowest eigenmodes, but that is not always the case [23, 24].

Thus, the main issue of the present work is to analyze the heating and mixing performances in a realistic mixer of simple geometry and, in particular, to study the effect of wall rotation on the enhancement of heat transport in the whole fluid domain. This crucial effect of wall on the mixing efficiency has been recently highlighted by Gouillart *et al.* [25, 26] for the homogenization of concentration in a 2D closed flow environment.

This article is organized as follows: in section 2, we present the problem, the geometrical description of the mixer, the fluid properties and the flow parameters. We also describe the different types of stirring protocols used to study the performance of the mixer for heat transport. The section ends with a presentation of the governing equations. In section 3, the numerical methods used to perform the simulations are described; in section 4, the mixing and energy indicators defined to quantify the efficiency of heat transport and homogenization are presented. All the results are detailed and discussed in section 5. At first, different flow topologies resulting from the choice of the stirring protocol imposed on the walls are shown,

and their incidences on mixing and heat transport are given. The results are also analyzed with the help of temperature probability distribution functions (PDFs), which are very useful in globally characterizing the homogenization of temperature in time. We show the existence of recurrent patterns of the temperature fields and explain them in terms of thermal strange eigenmodes. We also analyze the temporal evolution of the temperature gradients in the fluid domain. We conclude the section with a study of the effect of rod eccentricity. Finally, in section 6, concluding remarks are drawn and some perspectives for future work are given.

2. Problem statement

2.1. Geometrical description: the two-rod rotating mixer

A sketch of the studied mixer is presented in Figure 1. It is composed of two circular rods of equal radii, which are maintained vertically inside a cylindrical tank (a bounded domain). The tank and the rods are heated and can rotate around their respective revolution axis. This geometry is similar to the two-roll-mills studied in the literature by Price *et al.* [27] ; however, in our case, the outer cylinder has the ability to rotate. The rotation of the outer cylinder induces important consequences for the flow and mixing properties that will be explained later.

The geometry of the flow domain is characterized by two dimensionless parameters: the ratio of the radii of the rod and the cylindrical tank $(R_1 \; or \; R_2)/R_3$, and the dimensionless eccentricity $e = \varepsilon/R_3$. The geometrical parameters are set to $(R_1 \; or \; R_2)/R_3 = 1/5$ and a range between 0.35 and 0.60 for e ($R_1 = R_2 = 10 \; mm$, $R_3 = 50 \; mm$ and an eccentricity of $\varepsilon = 25 \; mm$ for the standard case study). In section 5.4, we will investigate the influence of variable eccentricity on thermal mixing.

The rods and the tank rotate alternately or with a continuous modulation of velocities. They can also have different directions of rotation.

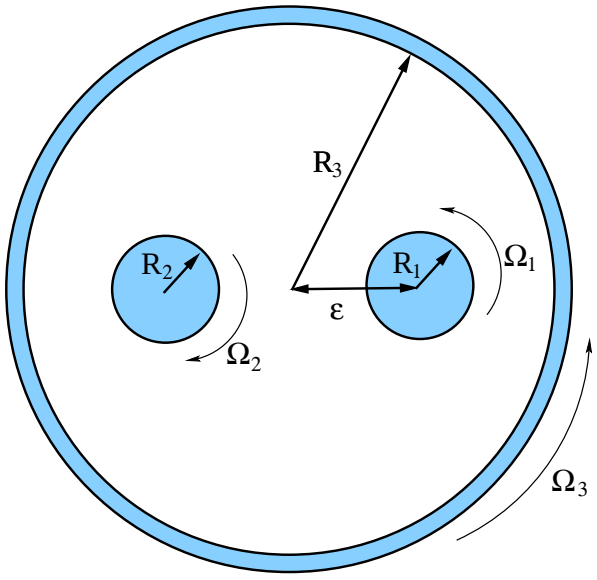

Figure 1: Sketch of the two-rod mixer.

The classical eccentric cylinder geometry studied in the past [5, 6, 7, 8] produced a large recirculation bubble, which could not be avoided even with a careful choice of stirring protocols. In contrast, the two-rod mixer [28] studied here is suitable to obtain full chaotic flow without KAM regions.

2.2. Fluid properties and flow parameters

The fluid considered in this study has the thermophysical properties listed in Table 1.

Dynamic viscosity (μ)	1.5 $Pa.s$
Density (ρ)	990 $kg.m^{-3}$
Thermal conductivity (k)	0.15 $W.m^{-1}K^{-1}$
Specific heat (c_p)	1000 $W.kg^{-1}K^{-1}$
Prandtl number (Pr)	10^4

Table 1: Fluid properties.

This fluid is Newtonian and has a high Prandtl number of $Pr = 10^4$. Considering these properties, the thermal diffusivity a is equal to 1.515×10^{-7} $m^2.s^{-1}$. The maximum angular wall velocities are fixed to: $\Omega_1 = \Omega_2 = 30$ rpm for the rods and $\Omega_3 = 6$ rpm for the outer tank. The tangential wall velocity is then the same, and equal to $U = 31.41$ $mm.s^{-1}$. A characteristic Reynolds number for this flow can be evaluated as:

$$Re = \frac{\rho\ U \cdot 2 \cdot (R_3 - R_1)}{\mu} = 1.66 \tag{1}$$

The walls of the rods and tank are kept at a constant *hot* temperature of T_{hot}. The initial uniform temperature of the fluid (before heating) is set to a *cold* temperature T_{cold}. We define the dimensionless fluid temperature as:

$$T^* = \frac{T - T_{cold}}{T_{hot} - T_{cold}} \tag{2}$$

Therefore, $T^*_{cold} = 0$ and $T^*_{hot} = 1$ and the maximum temperature difference between the walls and the fluid is always 1. The heated walls play the role of a variable heat source that is continuously dissipated in the 2D modulated flow field. This is a specific situation, not usually encountered when dealing with the scalar dissipation of concentration in a 2D velocity field. The Dirichlet boundary condition imposed to the walls implies that during the mixing of the fluid in the tank, the parietal fluxes will change along the walls as well as with time depending on the local flow conditions.

The other important dimensionless parameter for this non-isothermal mixing problem is the Péclet number, Pe = Re Pr. The Péclet number can be seen as the ratio of thermal diffusion time τ_{td} over advection time τ_{ad} for the scalar temperature. The limit Pe = 0 corresponds to the pure diffusion case. In our case, Pe is large (1.66 10^4 and then τ_{td} is $16,600$ times greater τ_{ad}); hence, the need to speed-up the mixing of temperature scalars is clearly demonstrated.

2.3. Stirring protocols

Chaotic mixing is produced here by varying in time the angular speed of the circular rods and the tank using a sine-squared waveform. The stirring protocols studied can be defined by two parameters: the respective direction of rotation between the rods and cylindrical tank, and the duration of the time periodic modulation. Other parameters, such as the ratio between the maximum velocities of the rod and cylindrical tank, and the amplitude of the angular velocity modulation, are not considered in this work. The three possible stirring configurations corresponding to the different flow topologies are specified in Table 2. The symbol (+) indicates a counter-clockwise direction and (−), a clockwise direction.

Stirring configuration	Rod 1	Rod 2	Tank
1	(+)	(−)	(+)
2	(+)	(+)	(+)
3	(−)	(−)	(+)

Table 2: The three possible stirring configurations related to the sign of angular velocity.

For chaotic flows, two types of temporal modulation are considered for the stirring protocols: a continuous one (a sine-squared modulation of wall velocities) and a non-continuous one (the rods are stopped together for half a period, during which time the outer cylinder is rotating; for the next half-period the contrary is considered). These stirring protocols are illustrated in Figure 2. The maximum angular velocity is the same for the two types of modulation. The rods and the cylinder tank follow sine-squared modulations as defined by equations 3 (here for a modulation period $\tau = 30\ s$):

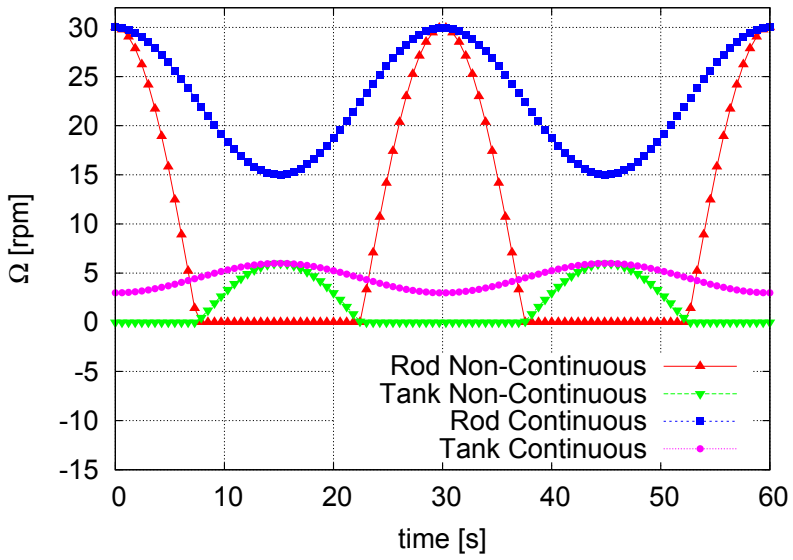

Figure 2: Temporal modulation of the angular velocities of the rods and tank for continuous and non-continuous stirring cases. Here the modulation period, τ, is 30 s.

Non-continuous case:

$$\begin{aligned} \Omega_{1,2} &= 30 - 60\sin^2(\tfrac{\pi t}{\mathcal{T}}) \quad \text{if} \quad \Omega_{1,2} < 0 \quad \Rightarrow \Omega_{1,2} = 0 \\ \Omega_3 &= 6 - 12\sin^2(\tfrac{\pi t}{\mathcal{T}} + \tfrac{\pi}{2}) \quad \text{if} \quad \Omega_3 < 0 \quad \Rightarrow \Omega_3 = 0 \end{aligned} \tag{3}$$

Continuous case:

$$\begin{aligned} \Omega_{1,2} &= 30 - 15\sin^2(\tfrac{\pi t}{\mathcal{T}}) \\ \Omega_3 &= 6 - 3\sin^2(\tfrac{\pi t}{\mathcal{T}} + \tfrac{\pi}{2}) \end{aligned}$$

It was common practice in the chaotic mixing process design to introduce a temporal modulation to the velocity of movement of mixer walls, which generally enhanced the efficiency of mixing. But often, the alternate rotation was not investigated.

In this work, the modulation period was varied from 15 to 100 s. For a modulation period of 15 s, the Strouhal number is typically on the order of $St = 0.34$. The Strouhal number is defined as:

$$St = \frac{2 \cdot (R_3 - R_1)}{U_{moy} \cdot \tau} \tag{4}$$

with $U_{moy} \approx 0.5\, U$. Considering this value, we can notice that this flow does not satisfy the quasi-steady hypothesis. As a consequence, in our modeling of the flow we need to account for inertial effects.

2.4. Governing Equations

The evolution of the scalar temperature transported in an incompressible laminar flow of a Newtonian fluid is described by the advection-diffusion equation written in its integral form:

$$\frac{\partial}{\partial t}\int_V \rho c_p T \, \mathrm{d}V + \int_S \rho c_p T \vec{U} \cdot \vec{n} \, \mathrm{d}S = \int_S k \vec{\nabla} T \cdot \vec{n} \, \mathrm{d}S \tag{5}$$

where k is the thermal conductivity. The integration is over a volume V surrounded by a surface S, which is oriented by the outward unit normal vector $\vec{n}$. As indicated before, the fluid is initially at a uniform cold temperature T_{cold}, and during the process the walls are maintained at a uniform hot temperature T_{hot} (Dirichlet condition). The velocity field of the flow $\vec{U}$ is obtained by resolution of the unsteady Navier-Stokes equations:

$$\int_S \vec{U} \cdot \vec{n} \, \mathrm{d}S = 0 \tag{6}$$

$$\frac{\partial}{\partial t}\int_V \rho \, \vec{U} \, \mathrm{d}V + \int_S \rho \, \vec{U}\vec{U} \cdot \vec{n} \, \mathrm{d}S = \int_V -\vec{\nabla} p \, \mathrm{d}V + \int_S \overline{\overline{\tau}} \cdot \vec{n} \, \mathrm{d}S \tag{7}$$

where $\overline{\overline{\tau}}$ is the viscous stress tensor. Here, the full Navier-Stokes equations are solved in order to take into account the inertial effects that are induced by the accelerated or decelerated movement imposed on the walls. The evolution of the fluid velocity and temperature fields are obtained by a CFD method, described in the next section.

3. Numerical methods

Two-dimensional continuity and Navier-Stokes equations, as well as the energy conservation equation, are solved by means of a inhouse code called Tamaris. This code has an

unstructured finite volume framework that is applied to hybrid meshes. Variable values ($\vec{U}$, p and T) are stored at cell centers in a collocated arrangement. Cell shapes can be triangular or quadrilateral.

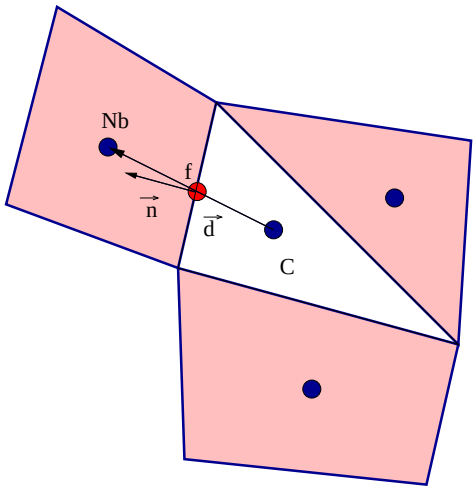

Figure 3: A computational cell and its neighbours.

To describe the discretization practice used in the code, we can write the above equations (5 and 7) in a unique generic form:

$$\frac{\partial}{\partial t}\int_V \rho\phi \, \mathrm{d}V + \int_S \rho\phi\vec{U}\cdot\vec{n} \, \mathrm{d}S = \int_S \Gamma\vec{\nabla}\phi\cdot\vec{n} \, \mathrm{d}S + \int_V S_\phi \, \mathrm{d}V \tag{8}$$

where S_ϕ is a source term. Spatial schemes approximating diffusive and convective fluxes are both second-order accurate. The discretization of the diffusion term is performed by approximating the surface integrals by a sum over all the cell faces f (see Figure 3):

$$\int_S \Gamma\vec{\nabla}\phi\cdot\vec{n} \, \mathrm{d}S = \sum_f \Gamma_f A_f (\overrightarrow{\nabla\phi})_f \cdot \vec{n}_f \tag{9}$$

In unstructured meshes, the normal gradient $(\overrightarrow{\nabla\phi})_f \cdot \vec{n}_f$ is decomposed into an implicit contribution that uses the values of f at the centers of the two cells sharing the face f (first term in the RHS of Eq. 10) and a non-orthogonality correction term treated explicitly by a deferred approach in order to preserve second order accuracy:

$$(\overrightarrow{\nabla\phi})_f \cdot \vec{n}_f = \frac{\phi_{nb} - \phi_c}{||\vec{d}||} + \overline{\overrightarrow{\nabla\phi}} \cdot \left(\vec{n} - \frac{\vec{d}}{||\vec{d}||}\right) \tag{10}$$

$\vec{d}$ is the vector joining the centers of the two cells (see Figure 3). The average gradient $\overline{\overrightarrow{\nabla\phi}}$ is interpolated from the gradients of these neighboring cells. The gradients of variables at the cell centers are computed by a second order least-square method that uses weighted values of ϕ at all the neighboring cells. Convection terms are also transformed in a sum over the faces

f composing the surface S:

$$\int_S \rho\phi\vec{U}\cdot\vec{n}\ \mathrm{d}S = \sum_f (\rho\phi A)_f \vec{U}_f\cdot\vec{n}_f \tag{11}$$

where face values ϕ_f require an appropriate interpolation. In the momentum equations, the blending difference scheme is used [29]. This scheme combines a second order accurate centered scheme with a low amount of upwind differencing to enforce the stability of the global scheme:

$$\phi_f = \phi_f^{upwind} + \beta(\phi_f^{centered} - \phi_f^{upwind})^{m-1} \tag{12}$$

where $m-1$ stands for the previous iteration. Here the weighting factor β is fixed at 0.95.

In the energy equation, special care was given to the face value interpolation in order to limit the numerical diffusion introduced, while preserving a strict boundedness. For this purpose the Normalized Variable Diagram (NVD) Gamma high resolution scheme of Jasak *et al.* [30] is used. This scheme introduces a smooth transition between centered and upwind differencing, depending on the local variation of the variable. This property is important for our study since we need to evaluate the efficiency of the heat advection mechanism in the absence of the numerical diffusion effect that may overshoot the thermal conduction role. Pressure-velocity coupling is ensured by the SIMPLE algorithm [31], while the mass fluxes at the cell faces are evaluated using the Rhie-Chow interpolation [32] to avoid pressure checkerboarding. Unsteady computations are advanced in time by the implicit three time step Gear's scheme that ensures second-order accuracy. At each iteration, the discretization technique presented above leads to the creation of a linear system with a non-symmetric sparse matrix for each variable. These linear systems are solved by means of an ILU preconditioned GMRES solver using the implementation of the IML++ library [33]. After a grid size-dependence study, a mesh of 9944 computational cells is adopted. This mesh was generated by the open-source software Gmsh [34] and is shown in Figure 4, where the use of regular quadrilateral cells near the walls to enhance the resolution of the boundary layers is noticeable. More details about the sensitivity of the results to the grid size as well as code validation are given in our recent paper [28].

4. Mixing and energy indicators

As mentioned by Finn *et al.* [35], a large variety of computational mixing measures exist. Many different criteria by which the quality of the mixing (with heat transfer or chemical reaction) may be evaluated will depend upon the application of interest. In order to characterize the efficiency of heat transfer by chaotic mixing, we introduce different mixing indicators, which are monitored throughout the evolution of the process. The first one is the mean temperature T_m^* of the fluid, which represents the energy extracted from the walls:

$$T_m^* = \frac{1}{\sum_c A_c}\left(\sum_c A_c T_c^*\right) \tag{13}$$

where the summation is made over all 2D computational cells c of area A_c. Indeed, this mean temperature evolution can be seen as an indicator of the ratio of the total energy supplied to

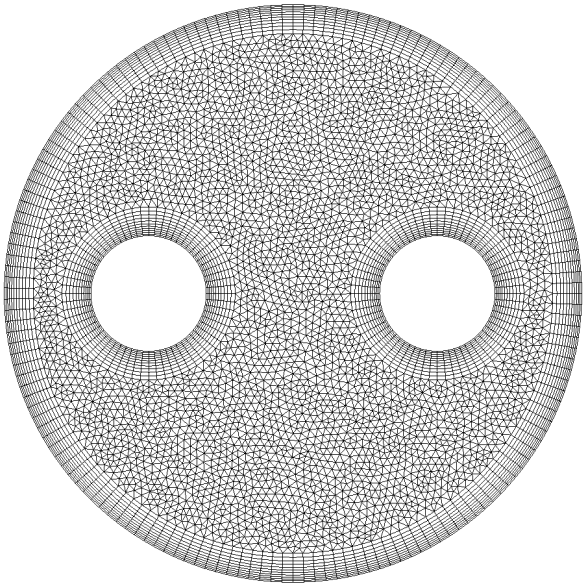

Figure 4: Computational mesh of the mixer.

the fluid from time 0 to t:

$$\begin{aligned} E(t) &= \int_{V_{tank}} \rho c_p (T(t) - T_{cold}) \mathrm{d}V = \rho c_p \left(\int_{V_{tank}} T(t) \mathrm{d}V - T_{cold} V_{tank} \right) \\ &= \rho c_p V_{tank} (T_m(t) - T_{cold}) \end{aligned} \tag{14}$$

As a consequence, the mean temperature is asymptotically bounded by the fixed temperature imposed on the walls (i.e., T_{hot} or 1 for non-dimensional temperature). The second mixing efficiency indicator is the standard deviation σ of the fluid temperature, which accounts for the level of homogenization of the scalar temperature inside the 2D tank:

$$\sigma = \left[\frac{1}{\sum_c A_c} \sum_c \left(A_c (T_c^* - T_m^*)^2 \right) \right]^{\frac{1}{2}} \tag{15}$$

Efficient thermal mixing requires good values for both of the aforementioned indicators (i.e., T^* near 1 and σ near 0). In order to compare several stirring protocols on the basis of these two indicators, it is useful to introduce a new indicator that combines the two effects:

$$A_{T\sigma} = \frac{1}{t_{final}} \int_0^{t_{final}} \frac{T_m^*}{\sigma} \, \mathrm{d}t \tag{16}$$

Then, for an efficient stirring protocol, $A_{T\sigma}$ must tend toward a high value. While the T_m^* and σ are unsteady indicators that evolve during the mixing process, $A_{T\sigma}$ is a single value that characterizes the whole process or at least during a period of t_{final}. This duration is chosen in such a way that, for all the studied stirring processes, T_m^* exceeds 0.95.

5. Results and discussion

5.1. Flow topologies and the effect of stirring protocols

In order to analyze the flow topologies involved in this mixer, we first present the flows obtained without modulation of the magnitude of the angular velocity. For the three stirring configurations discussed (cf. Table 2), we plotted the steady-state streamline topologies with and without the rotation of the outer cylinder.

From the plots of Figure 5 (a), (b) and (c) showing the steady streamline flow topologies, we can observe respectively:

- (a) Two stagnation points inside the fluid located towards the outer cylindrical wall on the vertical axis, seven separatrices, four parabolic points on the wall of the outer cylinder, counter-rotating closed streamlines around the rods, and four small vortices.
- (b) One stagnation hyperbolic point located at the centre of the tank, four separatrices, four parabolic points on the wall of the outer cylinder, co-rotating closed streamlines around the rods, and two large vortices. This configuration corresponds to the one shown in the paper of Price *et al.* [27] concerning a study of a family of two-roll-mill flows.
- (c) Closed streamlines along the wall of the cylindrical tank as in case (b), a hyperbolic stagnation point at the center of the tank, two large vortices, two separatrices around the vortices, two parabolic points on the wall of each rod and located on the vertical axis of symmetry of the rod, and two separatrices that join the wall rods.

In the lower half of Figure 5, the outer cylinder rotates and closed streamlines are always present in a layer near the wall regardless of the stirring configuration. This layer is thicker for stirring configuration 2 (Fig. 5 (e)), corresponding to co-rotation of the rods and cylinder.

When the rods and outer cylinder rotate steadily at the same time (Fig. 5 (d), (e) and (f)), the stagnation points observed on the walls in cases (a), (b) and (c) of the same figure disappear. We know from dynamical system theory that chaotic mixing will appear from the break-up of the separatrix, which dynamically separates regions of confined closed streamlines. A separatrix defines a heteroclinic trajectory that relies on two fixed (stagnation) points in the dynamical system terminology. Through the introduction of time-periodic perturbations, this heteroclinic connection is broken into two manifolds (one stable and the other unstable) that intersect transversely and give rise to what is called a heteroclinic tangle. The break-up of the separatrix occurs in our case when the rods and tank alternate their rotation. As a consequence, each stagnation point located on a wall is interesting because it defines the starting point for separatrix emanation. We will see later that the presence of these parietal fixed points play a key role in the extraction of heat from the walls. The fixed wall temperature imposed on all of the solid boundaries acts as a source for the evolution of the scalar; thus, the mean temperature will not be constant in time but will evolve asymptotically from $T_m^* = 0$ to $T_m^* = 1$ (the whole fluid is at the wall temperature). This behavior is shown in Figure 6 for stirring configuration 3 and three wall velocity modulation conditions: non-modulated, continuous and non-continuous (see Figure 2). In comparison, if we had considered the evolution of a material of dye for the same mixing process, the mean value of the dye concentration field would have been constant.

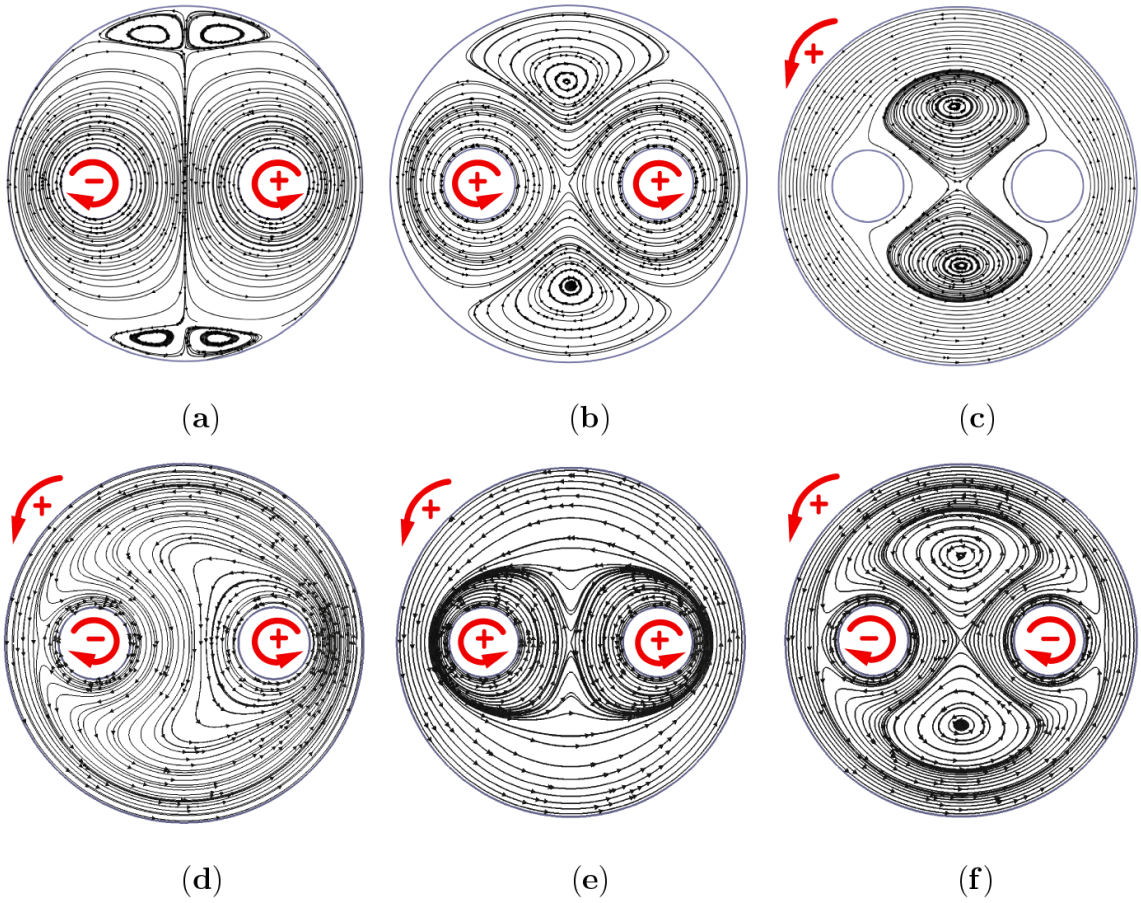

Figure 5: Generic steady-state streamline flow topologies. Upper half: without rotation of the outer cylinder: (a) counter-rotation and (b) co-rotation of the rods and (c) rotation of the outer cylinder tank without rod rotation. Lower half: with rotation of the outer cylinder for the stirring configurations 1 (d), 2 (e) and 3 (f) given in Table 2 (from left to right).

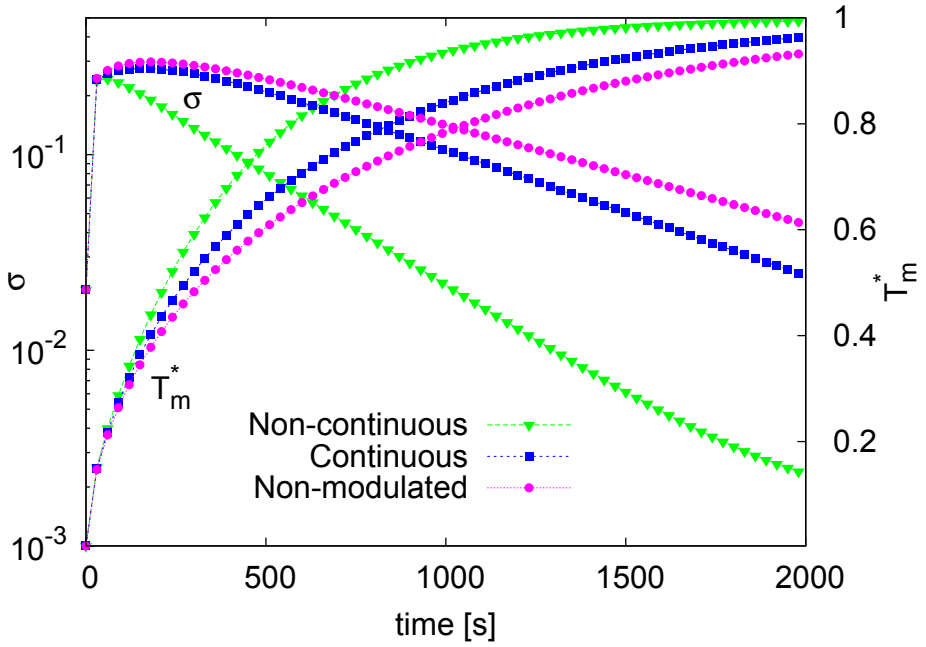

Figure 6: Temporal evolution of the standard deviation and mean value of the temperature for stirring configuration 3 and three wall velocity modulation conditions: non-modulated, continuous and non-continuous (see Figure 2).

From the temporal evolution of the standard deviation and mean temperature shown in Figure 6, it is evident that a non-continuous modulation of the velocity field enhances the mixing efficiency. After a transition time, the standard deviation of the temperature field decays exponentially for each modulation case; however, the decay rate is much higher for the non-continuous modulation condition (about a decade of difference on σ at 1500 s). While the temperature contrast decays exponentially, the mean temperature increases asymptotically towards the wall temperature $T^* = 1$. This behavior is easily understandable when we observe the temperature fields shown in Figure 7 for the three cases of angular velocity wall modulation. After several periods (t = 120 s), we find that only the non-continuous modulation condition avoids the persistence of large, non-heated zones. The temperature fields of non-modulated and continuously modulated cases are quite similar and follow very well the closed streamlines observed in Figure 5 (f). Moreover, these closed streamlines define a barrier for the evolution of the scalar towards the interior of the cylinder tank. Indeed, if the temperature difference is confined in a relatively large boundary along each wall, both the temperature gradient normal to the wall and the heat flux will decrease. Thus, the efficiency of the whole heat exchange will be reduced. In the case of non-continuous modulation, four parabolic points appear along the wall when the tank is stopped (see Figure 5(b)). It is from these parabolic points that strips of hot fluid will be pulled out from the wall. In Figure 7(c), it is evident that two of these points are diametrically opposed on the wall of the tank. At this time ($t = 120$ s), the tank has been at rest since 15 s.

This phenomenon of heat extraction from the walls for non-continuous stirring protocols is also clearly evident from Figure 8, which present simultaneous portraits of streamlines asso-

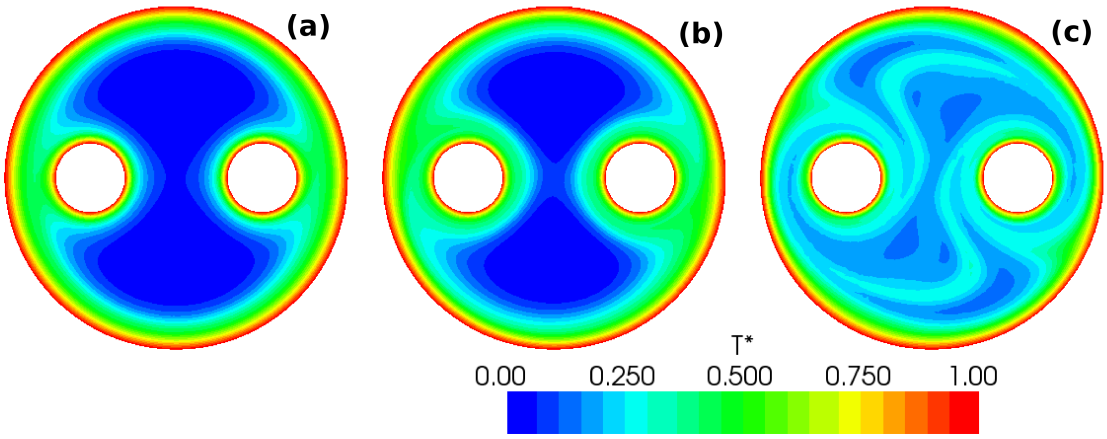

Figure 7: Dimensionless temperature field at $t = 120\ s$ for stirring configuration 3 and different flow modulations: (a) non-modulated, (b) continuous modulation and (c) non-continuous modulation (period of modulation $\tau = 30\ s$).

ciated with the corresponding temperature field. The hot heat fluid strips extracted from the tank (at 120 and 132 s) and rod walls (at 140 s) towards the interior of the mixer are clearly identifiable. Streamline portraits taken at different instants of the same period of modulation show crossings when superimposed. These conditions are generic for chaotic flow. As a consequence, the temperature field exhibits varied complex patterns. Recently Hertzsch *et al.* [36] have shown for a pulse source-sink chaotic system that the need to have a great transversality in streamline crossing is not always an optimal condition to improve global mixing. Hence, more theoretical studies are required to clearly understand the complex mechanism of the scalar gradient orientation with the strain axes in response to a disturbance of the velocity field imposed by the walls. This hovewer, is beyond the scope of the present work. In the following sections, only the condition of non-continuous modulation is investigated.

5.1.1. Effect of wall rotation direction and period length

In Figure 9, the three stirring configurations are compared over time for a modulation period of 15 s. We observe that the standard deviation of temperature decreases exponentially in each case. The relatively high standard deviation for stirring configuration 3 indicates the formation of large KAM islands in the mixer; the mixing is nevertheless good outside of these KAM regions.

In order to quantify the role of the modulation period length on mixing for the three stirring configurations, we plotted the composite indicator $A_{T\sigma}$ defined in section 4 for four modulation periods 15, 30, 60 and 100 s. We can observe in Figure 10 that this indicator reveals differences between stirring configurations mainly for low periods of modulation. An optimum seems to be a modulation period of 30 s for stirring configurations 1 and 2 and 60 s for stirring configuration 3. The latter combination is best even though configuration 3 gives, by far, the worst result at $\tau = 15\ s$. Thus, no clear preferential configuration can be deduced, but we can conclude that:

- short periods of modulation (about 15 s) should be avoided to achieve thermal mixing;

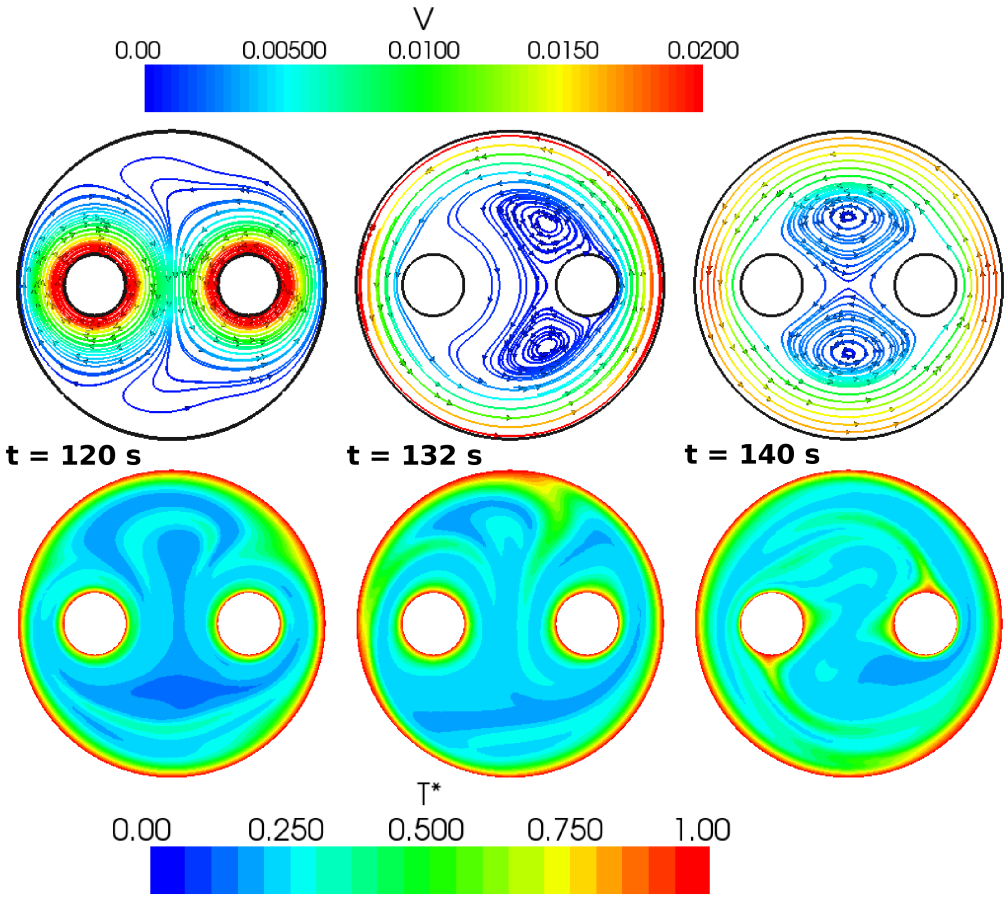

Figure 8: Evolution of flow patterns for stirring configuration 1 and non-continuous modulation of the wall velocities at different times during one period of the mixing process. Upper half streamlines. Lower half: dimensionless temperature fields. (Period of modulation $\tau = 30\ s$).

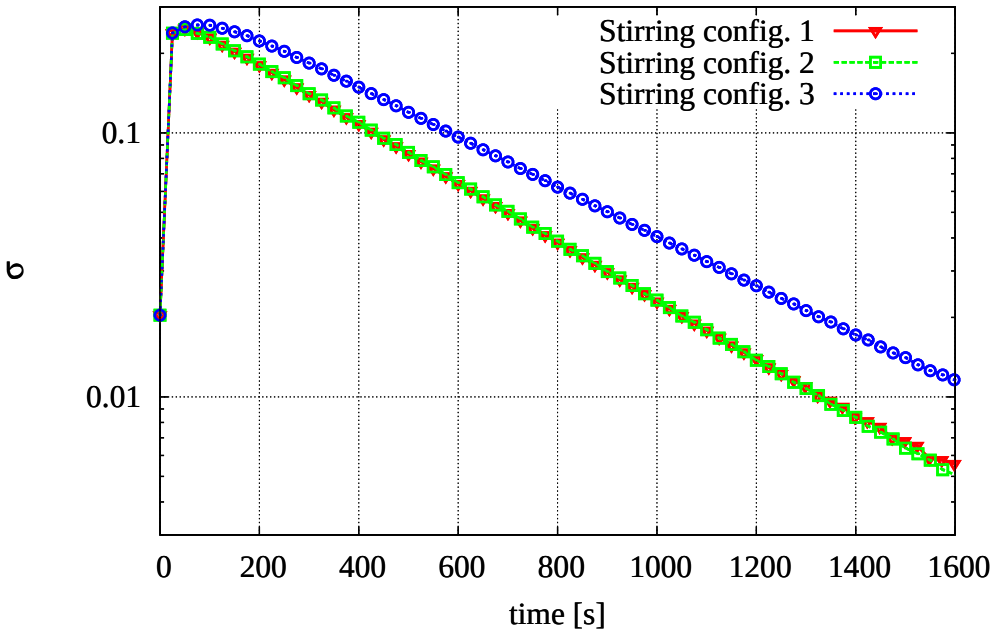

Figure 9: Standard deviation of temperature for the three stirring configurations of Table 2. The modulation period is $\tau = 15\ s$.

- configuration 1 does not give the best performance regardless of the period length;
- for a period length $\tau = 100\ s$, none of the configurations give optimum results.

Some explanations of these observations can be proposed by the examination of the evolution of the temperature field as the onepresented in Figure 8. For configuration 3 with a low period, the extracted hot fluid strips from the tank boundary during the rotation of the rods are not sufficiently long; therefore, these strips are brought back to the tank when the tank begins to rotate in the opposite direction. On the other hand, a period that is generally too long reduces the frequency of flow pattern alternation as well as that of stretching and folding operations.

5.2. Temperature Probability Distribution Functions (PDFs)

We focus here on the probability distribution functions of the dimensionless temperature T^* for the whole section filled by the fluid. Examples of such T^* fields are shown in Figures 7 and 8.

Figure 11 displays the PDFs at two different times for the three stirring configurations given in Table 2. For stirring configurations 1 and 2, which exhibit good mixing performances, a peak located is observed near the lowest temperatures. This peak moves in time to the right while its height increases. The shift of the PDF towards the right illustrates that the cold temperature disappears during the mixing process (and does so completely for good stirring configurations (configurations 1 and 2)). For stirring configuration 3, the PDF of the dimensionless temperature field remains quite flat even if the range of temperature is reduced. This result confirms the one observe in Figure 7 for the same stirring configuration.

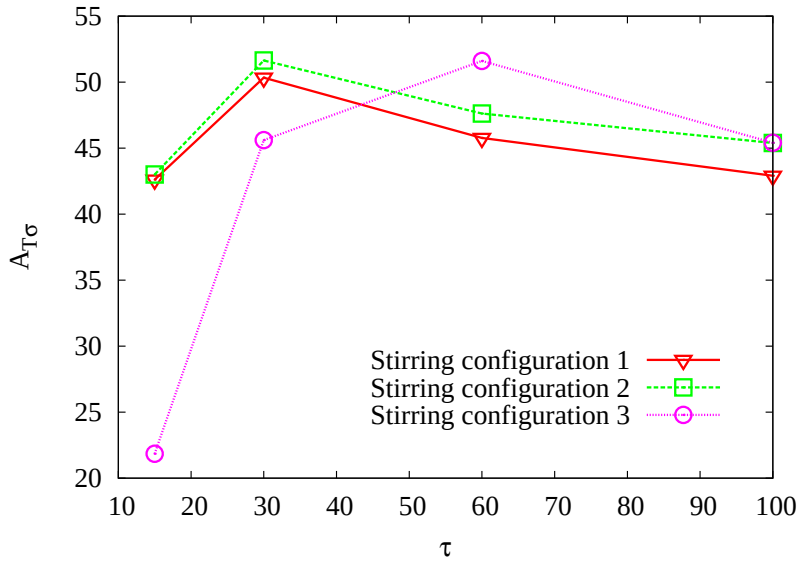

Figure 10: Composite mixing indicator $A_{T\sigma}$ as a function of the modulation period for a total mixing time of 1600 s.

An important feature of this thermal chaotic flow can be shown in Figure 12 by the PDFs of the rescaled dimensionless temperature:

$$X = \frac{T^* - T^*_m}{\sigma} \tag{17}$$

The PDFs, which are plotted for different times during the mixing process but at the same phase of the period, are superimposed; this is the signature of a strange eigenmode, which is characterized by the production of persistent patterns in the flow. These patterns arise from a combination of stretching, folding and thermal diffusion. The mechanism of their apparition and persistence will be detailed in the next section.

5.3. Thermal strange eigenmodes

The mechanism we investigate here is the spreading of temperature strips emerging from the walls in the bulk fluid. The flow has been chosen to produce chaotic mixing without the appearance of unmixed island (stirring protocol 2 and non-continuous modulation). The width s of a hot strip is imposed by an equilibrium between the stretching and folding and thermal diffusion. This width defines a length scale which is given by [26]:

$$s = \left(\frac{\alpha}{\lambda}\right)^{1/2} \tag{18}$$

where λ is a typical rate at which the equilibrium operates and represents a stretching rate. In our flow the stretching is not constant over the whole fluid domain, thus the widths of the hot strips evolve following local stretching rates. The effect of thermal diffusion can be understood by taking into account the average characteristic size s of a computational cell (near 0.7 mm) and the thermal diffusivity coefficient (see section 2.2). The thickness of a

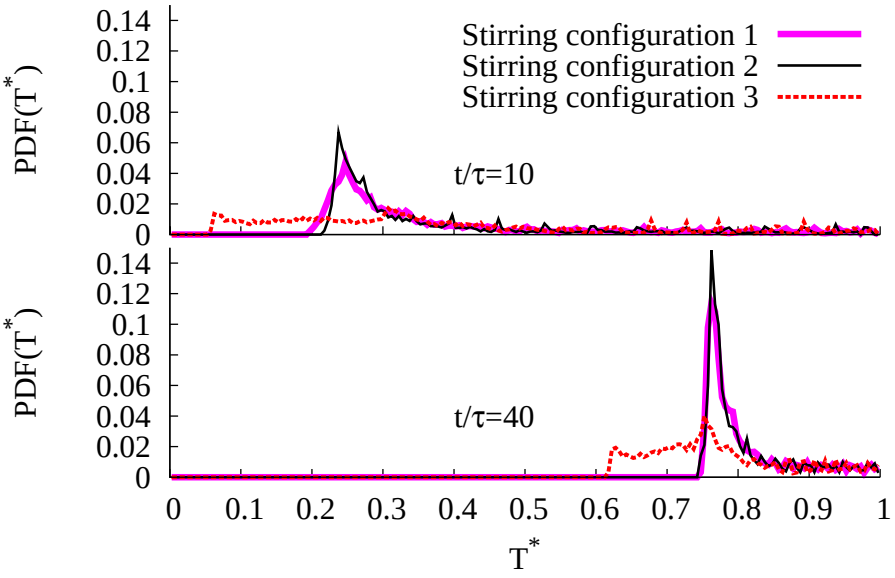

Figure 11: Probability distribution functions (PDFs) of T^* at two different times for $\tau = 15\ s$.

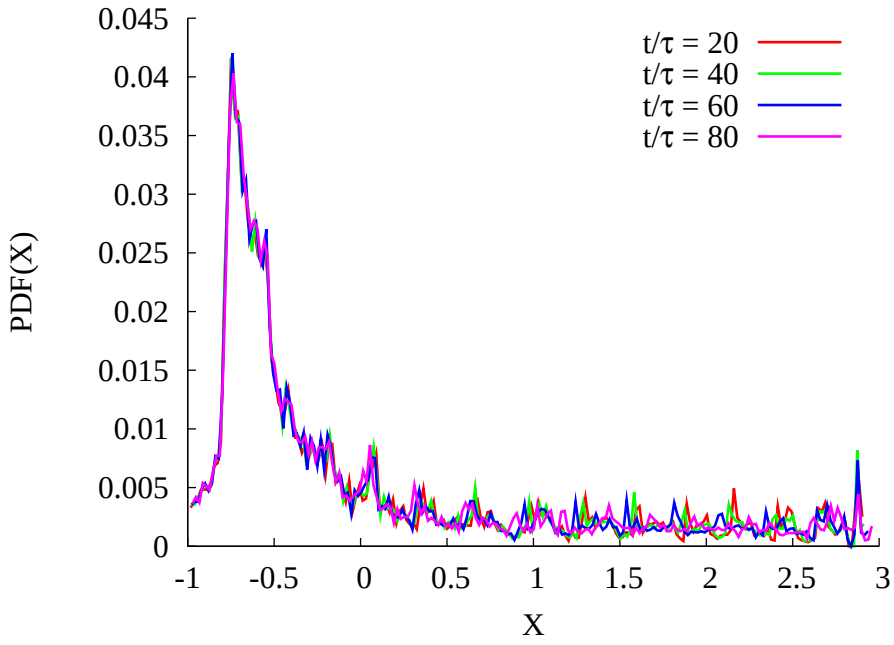

Figure 12: PDFs of the rescaled dimensionless temperature X for stirring configuration 2 at different times for $\tau = 15\ s$.

scalar strip that falls below this size will cease to be visible after a time $\frac{1}{\lambda} = \frac{s^2}{\alpha} \approx 3\ s$ that corresponds, for example, to a tenth of a period if $\tau = 30\ s$. Thus, the diffusive boundaries of the tracer strip interpenetrate rapidly to avoid the creation of very thin striations. The spatial structure of the temperature field is then smooth, which is due to the relatively high value of the thermal diffusivity and is also the reason why only relatively large temperature striations are observed. By comparison, the spatial structures of the concentration patterns generally present more lamellar structures due to a lowest value of mass diffusivity. This also is responsible for the nature of the pattern of the thermal strange eigenmode shown in the snapshots of Figure 13. The pattern is the same at each periodic time but the amplitude of the dimensionless temperature tends towards 1; this is also confirmed on the vertical cut-lines shown in Figure 14, where the temperature gradients correspondingly decrease. These curves were obtained by plotting the values of T^* along the vertical symmetry axis of the mixer.

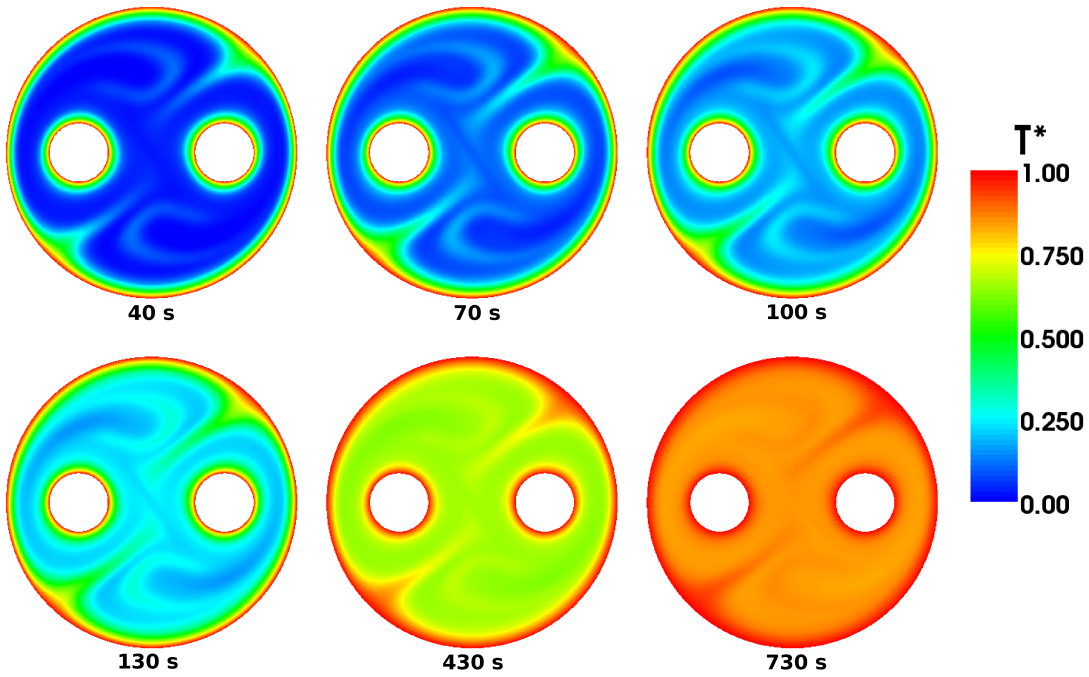

Figure 13: Snapshots showing the evolution of the temperature field towards a strange eigenmode for stirring configuration 2 and modulation period $\tau = 30\ s$.

In Figure 15, the temperature values for three of the snapshots of Figure 13 are rescaled between the T^*_{min} and T^*_{max} of each snapshot. With this scaling we observe that the patterns of the thermal eigenmode are exactly the same, which was not clearly obvious in Figure 13. Normalized vertical cut-lines of dimensionless temperature X (Eq. 17) are shown in Figure 16 for the same cases as those of Figure 14. The convergence to a thermal strange eigenmode is confirmed. The asymptotic transport properties of the time periodic flow are governed by this eigenmode.

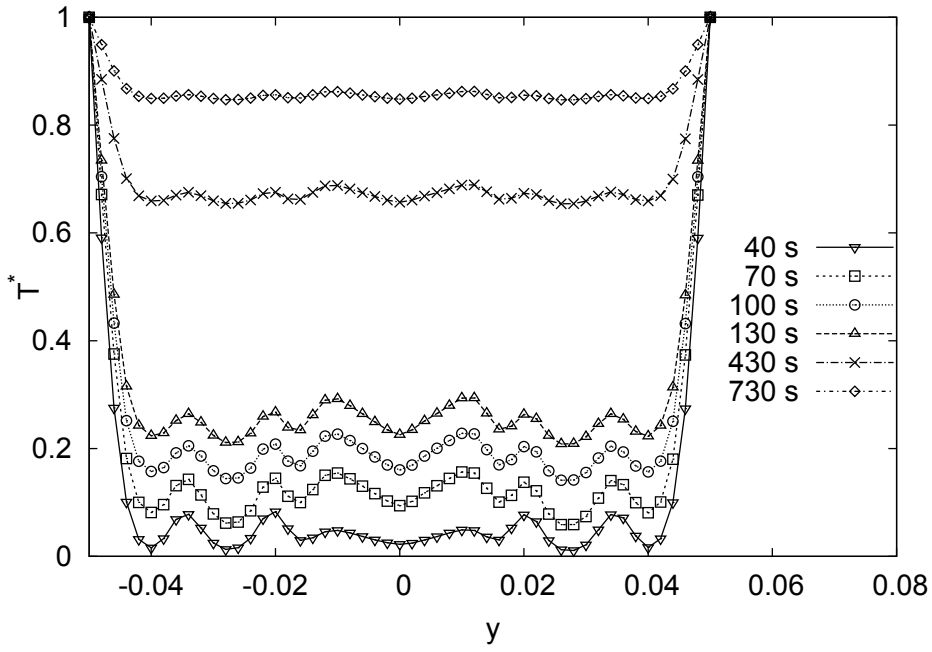

Figure 14: Vertical cut-lines of the dimensionless temperature at periodic times: 40, 70, 100, 130, 430 and 730 s (stirring configuration 2, $\tau = 30$ s).

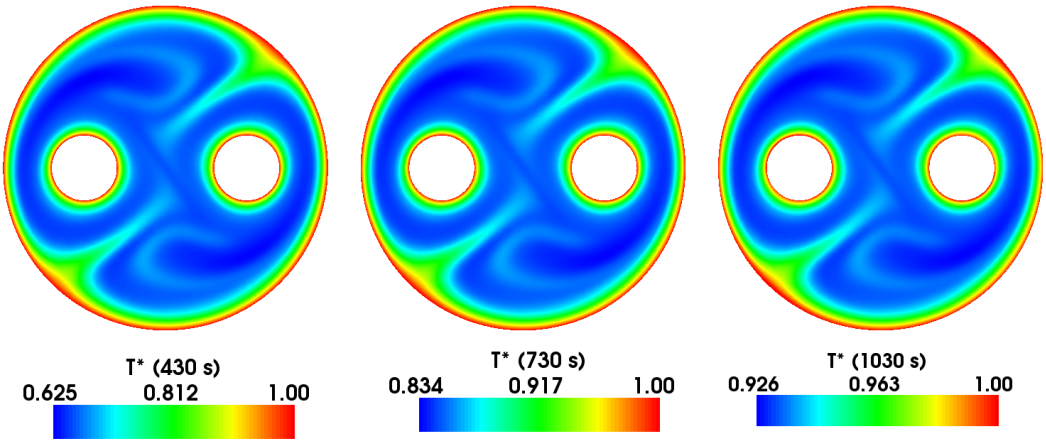

Figure 15: Snapshots showing the pattern of the strange thermal eigenmode for stirring configuration 2 and a modulation period $\tau = 30$ s. In these plots, the temperature scalars are rescaled between T^*_{min} and T^*_{max}.

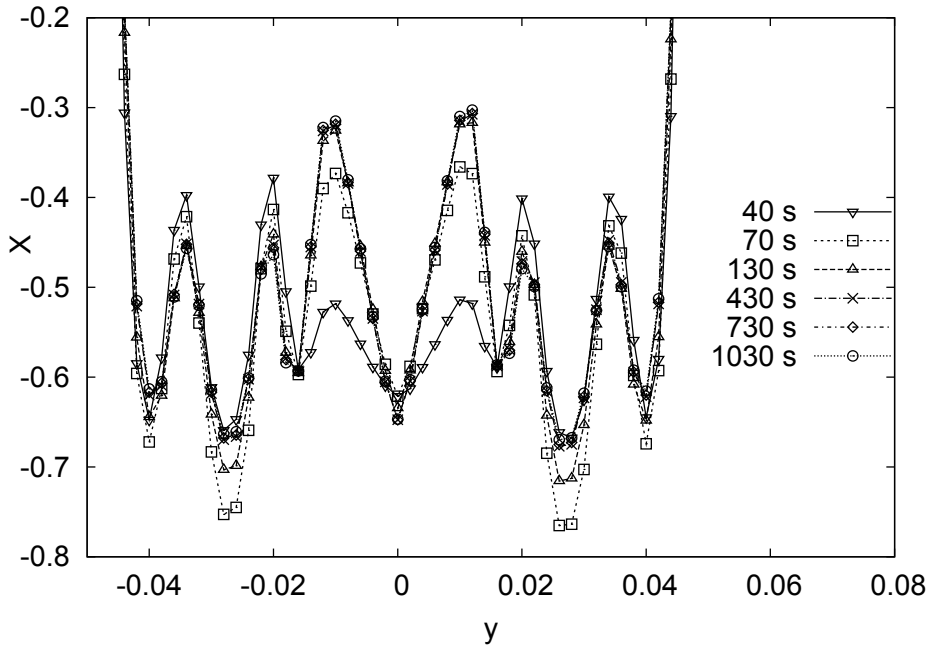

Figure 16: Normalized vertical cut-lines of the rescaled dimensionless temperature X at periodic times: 40, 70, 100, 130, 430 and 730 s (stirring configuration 2 and $\tau = 30$ s).

5.4. Effect of eccentricity

Figure 17 shows the difference of efficiency when changing the eccentricity. The largest eccentricity configuration ($\varepsilon = 30$ mm) gives the highest most probable value for the mean temperature but at the same time presents a broad tail at the left of the peak that extends towards the lower temperatures. This left tail is due to the persistence of non-heated zones, as clearly seen in Figure 18 (c).

The smallest eccentricity ($\varepsilon = 17.5$ mm) condition does not show a left tail (see Figure 17) but presents the lowest most probable value for the mean temperature. The intermediate rod eccentricity condition ($\varepsilon = 25$ mm) provides the best heating and temperature homogenization. This choice is a good compromise amongst the three cases.

5.5. Temperature gradient evolutions

In order to study and compare the evolution of the temperature gradients for different stirring protocols, we followed the temperature scalar dissipation indicator, which was defined as:

$$\chi_g = \frac{1}{S_{tot}} \int_{S_{tot}} \|\vec{\nabla} T^*\|^2 \, \mathrm{d}S = \frac{1}{\sum_c A_c} \left(\sum_c A_c \|\vec{\nabla} T^*\|_c^2 \right) \tag{19}$$

where S_{tot} is the total surface of the fluid in the mixer and A_c is the surface of a mesh element.

In Figure 19, we present the time evolution of this indicator for different stirring configurations. For two stirring protocols (stirring configuration 2 and stirring configuration 3 for $\tau = 60$ s) we observe perfectly exponential decreases. These cases correspond to the rapid

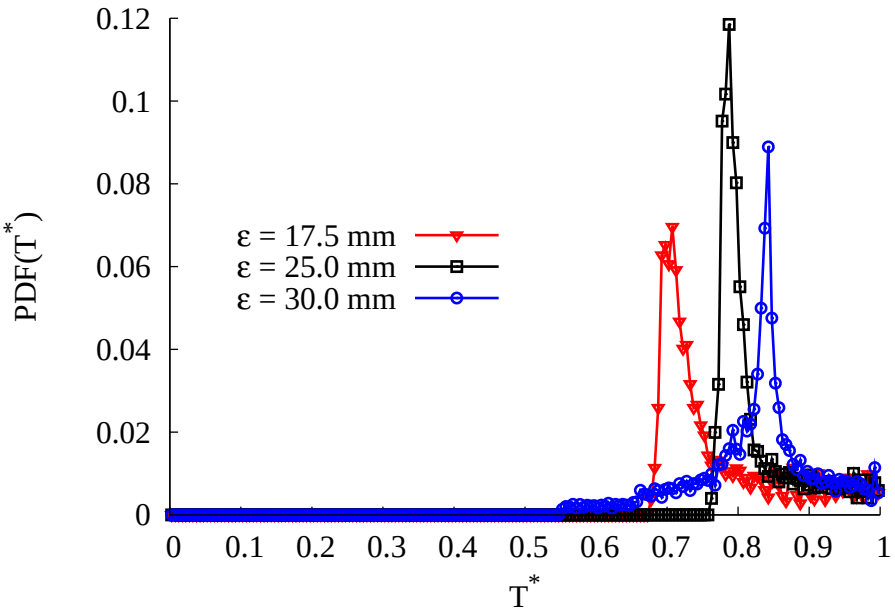

Figure 17: PDFs of non-dimensional temperature for stirring configuration 1 and three eccentricities: $\varepsilon = 17.5\ mm$, $\varepsilon = 25\ mm$ and $\varepsilon = 30\ mm$ ($\tau = 30\ s$).

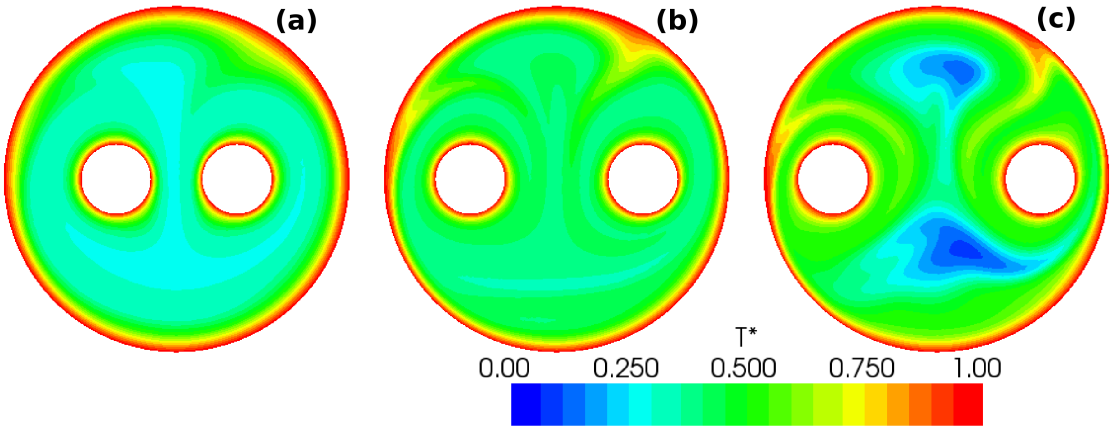

Figure 18: Dimensionless temperature fields for increasing mixer eccentricity at $t = 220\ s$ for stirring configuration 1. (a) $\varepsilon = 17.5\ mm$ (b) $\varepsilon = 25\ mm$ and (c) $\varepsilon = 30\ mm$ ($\tau = 30\ s$).

convergence of the temperature field to a recurrent spatial pattern characterized by a strange eigenmode (the patterns described in section 5.3 above). For the two other stirring protocols (continuous and the low modulation period of stirring configuration 3), the decay rates of the temperature gradients are slower than exponential. In the case of continuous rotation of the walls, the temperature gradients near the walls are imposed by the existence of the closed streamlines parallel to these boundaries. The temperature scalar transport evolves in these wall regions only by diffusion across streamlines, and the temperature gradient runs perpendicular to the streamlines. This mechanism has as a consequence the inhibition of thermal chaotic mixing; it is similar, in a certain way, to that observed by Gouillart *et al.* [25, 26] for the decay of the concentration of a scalar blob submitted to chaotic flow in a closed vessel with a no-slip boundary condition at the outer wall. However, in our case, continuous rotation of the wall is responsible for the non-asymptotic regime of thermal scalar gradient decay.

Contrary to the case of the dissipation of a concentration scalar (a blob of dye for example), which shows two consecutive phases, a phase of a creation of the gradients and a phase of their dissipation [37], only a phase for scalar dissipation exists for temperature scalar gradients. The main factor responsible for this difference is that thermal diffusion is much higher by comparison to molecular diffusion. Thus, thermal equilibrium is rapidly reached and temperature scalar striations are not conserved, contrary to concentration striations that remains in fluid and are thinner and numerous as well as stretching and folding operates. Nevertheless, the global structure of this field has a self-similar pattern. While the temperature field presents striations with the same spatial scale, even if their scalar magnitude is decreasing, the concentration field exhibits striations of decreasing spatial scale before the diffusion makes them disappear. Thus, there is a first phase of scalar gradient creation in the case of concentration mixing that is not present in the case of thermal mixing.

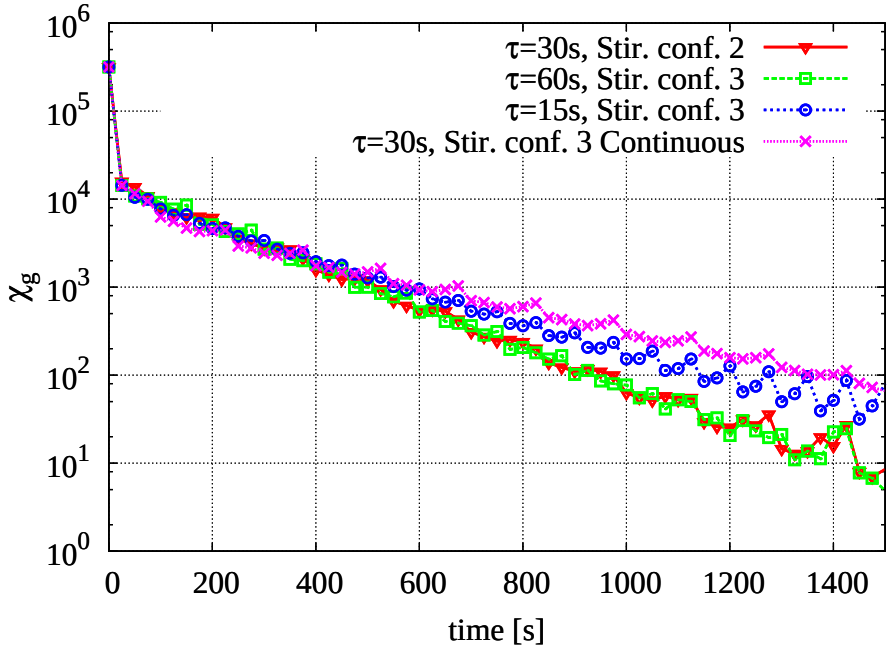

Figure 19: Evolution of the scalar temperature dissipation indicator for different stirring configurations.

6. Conclusion

We have numerically investigated the coupled mixing and heating performances induced by chaotic advection in a 2D two-rod mixer. Specific geometrical (eccentricity) and dynamical (stirring protocols, period length) parameters have been identified that promote a high degree of thermal mixing. We have shown the importance of the near wall flow topology for the development of efficient scalar temperature transport inside the mixer. For better understanding of the enhancement mechanism, different statistical tools and mixing and energy indicators have been used. A new composite indicator has been defined as the ratio of the mean temperature of the fluid (which represents the energy extracted from the walls) to the standard deviation of the fluid temperature (which corresponds to the level of homogenization of the scalar). We have also found that chaotic thermal mixing gives rise to singular recurrent spatial structures of the normalized non-dimensional temperature, while the mixing contrast tends to decay slowly with time. The main conclusion of our work is that maximizing heat transfer from the wall boundaries requires that the walls (i.e., tank or rods here) move alternately. In this way, one avoids the development of closed streamlines near the wall, which reduce the temperature gradients at the wall-fluid interfaces, and prevents the build-up of a wall-confined hot fluid zone. Continuous modulation of the wall is not sufficient; to produce effective chaotic mixing, the existence of stagnation points on the walls is necessary to create separatrices from which heteroclinic tangling can develop. Thus, the main advice to retain for industrial applications is the imperative to alternate the rotation of the stirring rods and the cylinder tank with non-continuous modulation (the rods are stopped when the cylinder tank rotates and vice-versa). Further studies will explore the constant wall heat flux boundary condition to study the influence of the thermodependence of the fluid physical properties on the thermal chaotic mixing. We will also address the problem of scalar temperature transport for rheologically complex fluids inside this thermal chaotic mixer.

References

[1] H. Aref, Stirring by chaotic advection, Journal of Fluid Mechanics 143 (1984) 1–21.

[2] H. Aref, The development of chaotic advection, Physics of Fluids 14 (2002) 1315–1325.

[3] J. Ottino, The kinematics of mixing: stretching, chaos, and transport, Cambridge University Press, 1989.

[4] F. Raynal, J. Gence, Energy saving in chaotic laminar mixing, International journal of heat and mass transfer 40 (14) (1997) 3267–3273.

[5] S. Ghosh, H. Chang, M. Sen, Heat-transfer enhancement due to slender recirculation and chaotic transport between counter-rotating eccentric cylinders, Journal of Fluid Mechanics 238 (1992) 119–154.

[6] V. Ganesan, M. Bryden, H. Brenner, Chaotic heat transfer enhancement in rotating eccentric annular-flow systems, Physics of Fluids 9 (1997) 1296–1306.

[7] A. Lefevre, J. Mota, A. Rodrigo, E. Saatdjian, Chaotic advection and heat transfer enhancement in Stokes flows, International Journal of Heat and Fluid Flow 24 (3) (2003) 310–321.

[8] J. Mota, A. Rodrigo, E. Saatdjian, Optimization of heat-transfer rate into time-periodic two-dimensional Stokes flows, International journal for numerical methods in fluids 53 (6) (2007) 915–931.

[9] H. Peerhossaini, C. Castelain, Y. Le Guer, Heat exchanger design based on chaotic advection, Experimental thermal and fluid science 7 (4) (1993) 333–344.

[10] A. Mokrani, C. Castelain, H. Peerhossaini, The effects of chaotic advection on heat transfer, International Journal of Heat and Mass Transfer 40 (13) (1997) 3089–3104.

[11] C. Chagny, C. Castelain, H. Peerhossaini, Chaotic heat transfer for heat exchanger design and comparison with a regular regime for a large range of Reynolds numbers, Applied Thermal Engineering 20 (17) (2000) 1615–1648.

[12] N. Acharya, M. Sen, H. Chang, Analysis of heat transfer enhancement in coiled-tube heat exchangers, International Journal of Heat and Mass Transfer 44 (17) (2001) 3189–3199.

[13] T. Lemenand, H. Peerhossaini, A thermal model for prediction of the Nusselt number in a pipe with chaotic flow, Applied Thermal Engineering 22 (15) (2002) 1717–1730.

[14] Y. Le Guer, E. Schall, A mapping tool using anisotropic unstructured meshes to study mixing in periodic flows, Chemical Engineering Science 59 (7) (2004) 1459–1472.

[15] C. Boesinger, Y. Le Guer, M. Mory, Experimental study of reactive chaotic flows in tubular reactors, AIChE Journal 51 (8) (2005) 2122–2132.

[16] S. Gibout, Y. Le Guer, E. Schall, Coupling of a mapping method and a genetic algorithm to optimize mixing efficiency in periodic chaotic flows, Communications in Nonlinear Science and Numerical Simulation 11 (3) (2006) 413–423.

[17] V. Kumar, M. Mridha, A. Gupta, K. Nigam, Coiled flow inverter as a heat exchanger, Chemical Engineering Science 62 (9) (2007) 2386–2396.

[18] V. Kumar, K. Nigam, Laminar convective heat transfer in chaotic configuration, International Journal of Heat and Mass Transfer 50 (13-14) (2007) 2469–2479.

[19] A. Yamagishi, T. Inaba, Y. Yamaguchi, Chaotic analysis of mixing enhancement in steady laminar flows through multiple pipe bends, International Journal of Heat and Mass Transfer 50 (7-8) (2007) 1238–1247.

[20] D. Lester, M. Rudman, G. Metcalfe, Low Reynolds number scalar transport enhancement in viscous and non-Newtonian fluids, International Journal of Heat and Mass Transfer 52 (3-4) (2009) 655–664.

[21] R. Pierrehumbert, Tracer microstructure in the large-eddy dominated regime, Chaos Solitons and Fractals 4 (6) (1994) 1091–1110.

[22] W. Liu, G. Haller, Strange eigenmodes and decay of variance in the mixing of diffusive tracers, Physica D: Nonlinear Phenomena 188 (1-2) (2004) 1–39.

[23] A. Pikovsky, O. Popovych, Persistent patterns in deterministic mixing flows, Europhysics Letters 61 (5) (2003) 625–631.

[24] O. Popovych, A. Pikovsky, B. Eckhardt, Abnormal mixing of passive scalars in chaotic flows, Physical review. E, Statistical, nonlinear, and soft matter physics 75 (3) (2007) 036308.

[25] E. Gouillart, N. Kuncio, O. Dauchot, B. Dubrulle, S. Roux, J. Thiffeault, Walls Inhibit Chaotic Mixing, Physical Review Letters 99 (11) (2007) 114501.

[26] E. Gouillart, O. Dauchot, B. Dubrulle, S. Roux, J. Thiffeault, Slow decay of concentration variance due to no-slip walls in chaotic mixing, Physical review. E, Statistical, nonlinear, and soft matter physics 78 (2) (2008) 026211.

[27] T. Price, T. Mullin, J. Kobine, Numerical and experimental characterization of a family of two-roll-mill flows, Royal Society of London, Proceedings Series A (2003) 117–135.

[28] K. El Omari, Y. Le Guer, A numerical study of thermal chaotic mixing in a two rod rotating mixer, Computational Thermal Science (2009) 1–12.

[29] J. Ferziger, M. Perić, Computational methods for fluid dynamics, Springer New York, 2002.

[30] H. Jasak, H. Weller, A. Gosman, High resolution NVD differencing scheme for arbitrarily unstructured meshes, International Journal for Numerical Methods in Fluids 31 (2) (1999) 431–449.

[31] S. Patankar, Numerical heat transfer and fluid flow Series in computational methods in mechanics and thermal sciences, Taylor & Francis, 1980.

[32] C. Rhie, W. Chow, Numerical study of the turbulent flow past an airfoil with trailing edge separation, AIAA Journal 21 (11) (1983) 1525–1532.

[33] J. Dongarra, A. Lumsdaine, R. Pozo, K. Remington, A sparse matrix library in C++ for high performance architectures, in: Proceedings of the Second Object Oriented Numerics Conference, 1994, pp. 214–218.

[34] C. Geuzaine, J. Remacle, Gmsh: a three-dimensional finite element mesh generator with built-in pre-and post-processing facilities, Accepted for publication in International Journal for Numerical Methods in Engineering.

[35] M. Finn, S. Cox, H. Byrne, Mixing measures for a two-dimensional chaotic Stokes flow, Journal of Engineering Mathematics 48 (2) (2004) 129–155.

[36] J. Hertzsch, R. Sturman, S. Wiggins, DNA Microarrays: design principles for maximizing ergodic, chaotic mixing, Small 3 (2).

[37] D. Rothstein, E. Henry, J. Gollub, Persistent patterns in transient chaotic fluid mixing, Nature 401 (6755) (1999) 770–772.